Available online at www.sciencedirect.com
ScienceDirect
Polymer 48 (2007) 6374–6383
polymer
www.elsevier.com/locate/polymer

Microstructural origin of physical and mechanical properties of ultra high molecular weight polyethylene processed by high velocity compaction

D. Jauffrès [a], O. Lame [a,*], G. Vigier [a], F. Doré [b]

[a] *MATEIS, INSA-Lyon, CNRS UMR5510, Bât. B. Pascal 7 Avenue Jean Capelle, F-69621 Villeurbanne cedex, France*
[b] *CETIM, 7 rue de la presse, BP802, F-42952 Saint Etienne cedex 9, France*

Received 28 June 2007; received in revised form 25 July 2007; accepted 26 July 2007
Available online 1 August 2007

Abstract

Ultra High Molecular Weight Polyethylene (UHMWPE) is a semi-crystalline polymer with exceptional wear and impact properties, but also a very high melt viscosity, owing to its extremely long chains. Therefore, UHMWPE is non-melt processable and its processing is long and expensive. However, a new process, High Velocity Compaction (HVC), allows processing UHMWPE within short processing times via sintering. Several high velocity impacts are applied to a powder-filled die to provide self-heating. The sintering is then obtained by local fusion/recrystallization. In this study, the physical and mechanical properties of UHMWPE processed by HVC are investigated. Ductile UHMWPE with a high modulus was obtained. The particular microstructure of the material resulting from the sintering by fusion/recrystallization has then been characterized. It appears that mechanical properties of HVC–UHMWPE are governed by the microstructure induced by processing conditions, and hence can be adjusted for a given application.

Keywords: Ultra high molecular weight polyethylene; High velocity compaction; Sintering

1. Introduction

Ultra High Molecular Weight Polyethylene (UHMWPE) is a linear polyethylene whose molar mass exceeds 3 000 000 g/mol. By comparison, classical High Density Polyethylene (HDPE) molar mass is generally below 300 000 g/mol. The properties and processing of UHMWPE have recently been reviewed by Kelly [1]. The extremely high molar mass of UHMWPE imparts to its outstanding wear resistance and impact toughness, better than any other polymer. Thanks to these properties and high biocompatibility, UHMWPE is widely used as a bearing surface in orthopedic implants (knee, hip, and shoulder implants). UHMWPE is also highly valued for several industrial applications requiring wear resistance, such as conveying systems. In addition, it is used to produce high strength fibers.

Processing UHMWPE is problematic due to its high molecular weight. It induces a very high melt viscosity that prevents UHMWPE from being processed by conventional melt processes (extrusion and injection molding). Therefore, processes inspired by powder metallurgy such as cold compaction followed by sintering [2], compression molding [3], or hot isostatic pressing [4] have been developed. Currently, the so-called ''as-polymerized'' or ''nascent'' powder, directly extracted from the polymerization reactor, is industrially processed by ram extrusion or compression molding. Both processes consist in applying elevated temperatures (above the melting point) and pressures to consolidate the powder into a bulk material. These processes are long (several hours) and expensive, thus limiting the use of UHMWPE to high performance applications.

High Velocity Compaction (HVC), first developed for ceramic and powder metallurgy, consists in applying high velocity impacts to a powder-filled die to form a green body that is sintered afterwards. HVC has been also

* Corresponding author. Tel.: +33 4 72 43 83 57; fax: +33 4 72 43 85 28.
E-mail address: olivier.lame@insa-lyon.fr (O. Lame).

0032-3861/$ - see front matter © 2007 Elsevier Ltd. All rights reserved.
doi:10.1016/j.polymer.2007.07.058

attempted to process polyamide powder at ambient temperature [5].

At CETIM (Technical Center – Saint Etienne, France), the HVC press has been adapted for compaction at elevated temperature. The use of elevated temperature is necessary to sinter a polymer powder by HVC. This technique allows processing semi-crystalline polymers without viscosity limitation, and appears to be well suited for UHMWPE. It has been shown that good sintering of semi-crystalline polymer powders is possible thanks to repeated impacts at a temperature close to, but below, the polymer melting point [6,7]. It has been assumed that the repeated impacts provoke a local melting at particle interface and that the welding of the particles would be provided by recrystallization of the melted material during cooling (Fig. 1).

Polyoxymethylene (POM) was the first polymer successfully processed by HVC [7]. ''Nascent'' POM powders, directly extracted from the polymerization reactor, were used. In the reactor, crystallization occurs simultaneously with polymerization, imparting to POM nascent powders a high crystallinity (~90%). This high ''nascent'' crystallinity is irreversibly lost after the first melting and POM crystallized from the melt exhibits a lower crystallinity (~70%). Contrary to conventional processing, HVC does not involve complete melting of the polymer and a large part of nascent high crystallinity is preserved. This is of major importance, as stiffness of semi-crystalline polymers is governed by crystallinity [8,9]. POM processed by HVC revealed to be at least 50% stiffer than injection molded POM [6,7]. However, HVC POM has a brittle behavior with only around 1% strain before rupture (occurring at ~50 MPa). It has been shown (especially, thanks to microscopic observation of crushed powder particles) that brittleness would be intrinsic to POM nascent powders, probably owing to the particular microstructure of nascent POM [7].

UHMWPE nascent powders are also highly crystalline because of simultaneous crystallization and polymerization, but do not present the drawback of being brittle.

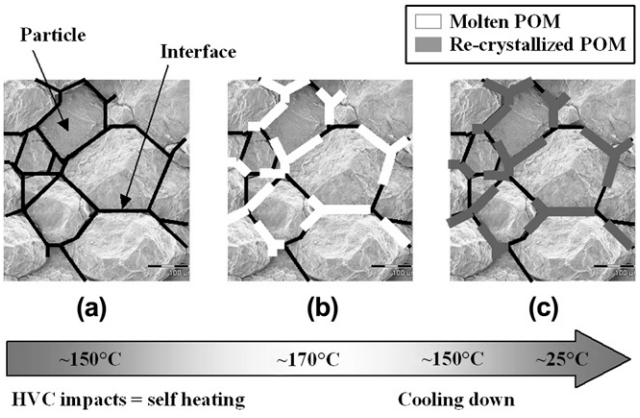

Fig. 1. Sintering mechanism of POM HVC. (a) Initial state. (b) Local melting at particle interfaces. (c) Recrystallization provides the welding of the particles from Ref. [7].

As a consequence, it has been considered to produce UHMWPE by HVC, in order to obtain a highly crystalline and stiff material. In addition, UHMWPE processed by HVC should be financially interesting thanks to short processing times and the possibility to produce simple parts (with a planar geometry) without additional machining.

This paper presents physical and mechanical characterizations of UHMWPE processed by HVC under different processing conditions. HVC UHMWPE properties are compared to conventionally processed UHMWPE ones and the influence of processing parameters is studied. The discussion aims to characterize the particular microstructure of HVC UHMWPE and to investigate the relationships between processing parameters, microstructure and mechanical properties.

2. Material and process

2.1. Nascent UHMWPE powder

A commercial nascent UHMWPE powder was used in this study: GUR 4113 produced by Ticona (Oberhausen, Germany). The powder particles, around 100 μm in size, present the particular nodular structure (Fig. 2) reported several times in the literature [1,10–13]. The viscosity average molecular weight of GUR 4113 is reported to be 3 900 000 g/mol by Ticona.

Nascent UHMWPE is characterized by a high crystallinity and a high melting point that are irreversibly lowered after melting/recrystallization. For nascent UHMWPE, crystallinity degrees in the range 60–75% and peak melting temperatures in the range 138–143 °C have been reported at conventional heating rates, while UHMWPE crystallized from the melt is approximately 50% crystalline and melts around 135 °C [14–16]. A melting peak at 142 °C and a crystallinity degree of 68% have been measured on GUR 4113. Particularly high melting temperature was first associated with the presence of chain extended crystal [15], but Tervoort-Engelen and Lemstra brought experimental evidence against this hypothesis and have proposed that the high melting temperature is due to a rapid annealing during differential scanning calorimetry [16]. More recent studies have suggested that the high melting stability originates in constrains in the amorphous phase created by simultaneous crystallization and polymerization [17–20].

2.2. HVC process

The several steps of HVC are schematized in Fig. 3. The temperature of the tools (die, upper punch and lower punch) is regulated at the chosen *processing temperature*. Before filling, the powder is pre-heated at this temperature. Then, after a pre-compaction step at 60 MPa, the upper punch is impacted up to 100 times by the HVC hammer, at precisely controlled compaction energy.

In the following, *total energy* refers to the energy of one impact multiplied by the number of impacts. *Total energy*

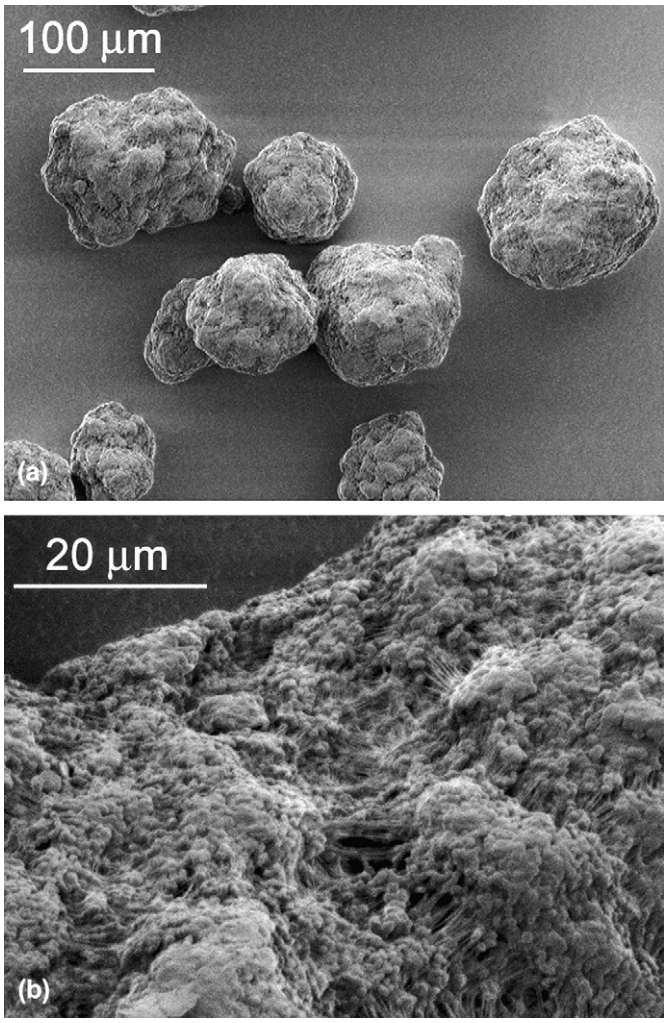

Fig. 2. Low voltage scanning electron microscopy observation of GUR 4113 powder. (a) Particles. (b) Nodular structure on particle surface.

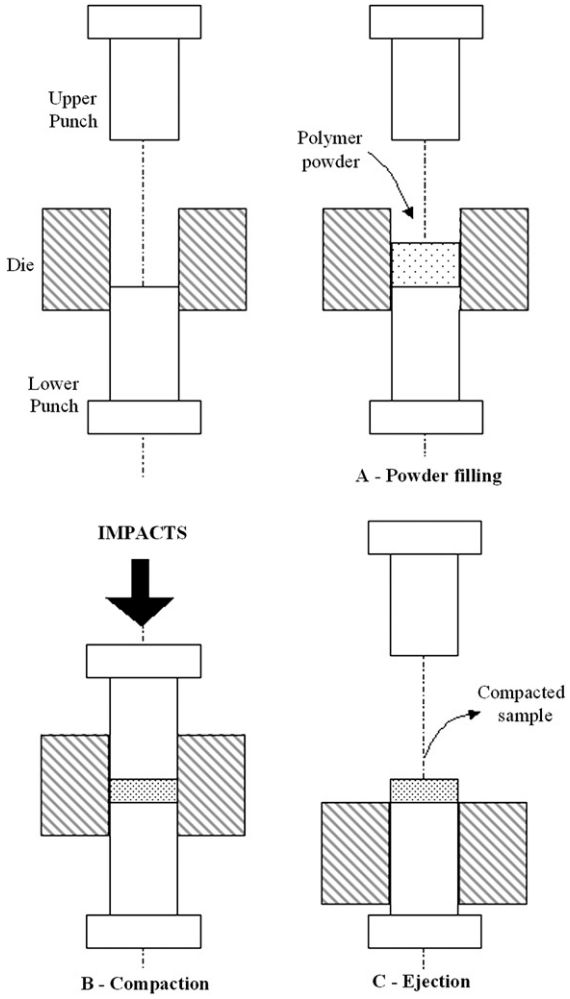

Fig. 3. Schematic representation of the three steps involved during HVC processing.

seems to be the relevant parameter: it has been observed that the same amount of energy brought by 25 impacts at 80 J/g or by 100 impacts at 20 J/g leads to the same result. The impact energy was fixed at 40 J/g, and different *total energies* were obtained by varying the number of impacts. Parameters (*processing temperature* and *total energy*) were chosen considering the recent results obtained on POM [7]. Temperatures were chosen between 115 °C (~30 °C under melting peak) and 125 °C (near melting onset temperature). For each temperature, UHMWPE was processed at *total energies* ranging from 800 J/g to 4300 J/g.

3. Characterization methods

3.1. Density measurements

Densities were obtained by weighting samples and determining their volume through the intermediary of Archimedes force. This method leads to a precision of $\pm 5 \times 10^{-3}$ g/cm^3.

For semi-crystalline polymers, density is often used to obtain the crystallinity degree [21]:

$$\Phi_c = \frac{\rho - \rho_a}{\rho_c - \rho_a} \tag{1}$$

$$X_c = \Phi_c \frac{\rho_c}{\rho} \tag{2}$$

where Φ_c is the crystal volume fraction, X_c the crystal weight fraction, ρ the material density, ρ_a the amorphous phase density and ρ_c the crystal phase density. For polyethylene, $\rho_a = 0.855$ g/cm^3 and $\rho_c = 0.999$ g/cm^3 [22]. Here, this method is not relevant to determine the crystallinity as it is strongly suspected that some samples are not fully dense. However, if the crystal weight fraction is obtained by another means it is possible to calculate theoretical density ρ_{theo} of the fully dense material, and hence to use density measurements to evaluate the sample porosity.

From Eqs. (1) and (2):

$$\rho_{theo} = \frac{-\rho_c \rho_a}{X_c(\rho_c - \rho_a) - \rho_c} \tag{3}$$

3.2. Differential Scanning Calorimetry (DSC)

The crystallinity was investigated by DSC technique. A Perkin Elmer DSC Pyris was used with a temperature ramp of 10 °C/min. A mass of 5 ± 1 mg was chosen and precautions were taken to ensure a stable sample specific surface, in order to keep a constant thermal transfer coefficient.

The classical method to determine the crystal weight fraction X_c consists in dividing sample melting enthalpy by crystal polymer enthalpy (given at equilibrium melting temperature). This method leads to slightly less elevated crystallinities than the ones obtained by density measurements [21,23]. As crystal weight fraction is used to calculate the theoretical density that is compared to measured densities in order to evaluate the porosity, it is needed to remove this discrepancy.

Kong and Hay introduced the so-called ''first law method'' [23] that leads to DSC crystallinity degrees consistent with density crystallinity degrees. This method, precisely described by Kong and Hay [23], was applied between 80 °C and 150 °C. The melting enthalpy of polyethylene crystal at 80 °C necessary for the calculation was determined to be 274 J/g using crystal and liquid specific heat data available in Polymer handbook [22].

Finally, crystallinity was obtained from DSC with a precision of ±0.01.

Consistency of theoretical density calculated from DSC crystallinity was checked on melt-recrystallized UHMWPE (assumed to be fully dense): the measured density is 0.935 ± 0.005 g/cm^3, while the theoretical density is 0.930 ± 0.010 g/cm^3.

3.3. Three-point bending tests

Mechanical properties were investigated by three-point bending tests. Bending test allows us to

- propose a criterion to distinguish easily ductile samples from brittle ones,
- measure Young's modulus with a good accuracy.

The bending specimens were 3 mm thick, 6 mm wide and 30 mm long. The distance between the two external contacts was 25 mm, and the strain rate was 5×10^{-4} s^{-1}. Initial Young's modulus was calculated from force and deflection measurements, in the small deformation hypothesis, according to ASTM D790 [24]. The precision was estimated to be ±0.1 GPa and an average value obtained over two or three tests is presented. After a significant deflection (~5 mm, which corresponds to more than 10% strain), specimens take a V-shape and force begins to drop. At this point, if the specimen has not already failed, the test is stopped and the specimen is considered as ''ductile''.

3.4. Tensile tests

In order to reach large deformation and obtain materials' ultimate properties, uniaxial tensile tests were performed on ductile samples. Tensile specimens had a rectangular cross-section of 1 mm × 5 mm and a gage length of 10 mm. A video-controlled testing system (VideoTraction® by Apollor) was used to measure true stress and true strain at a constant true strain rate of 1×10^{-3} s^{-1}. G'Sell et al. have developed this system; one can refer to their publication for more details [25].

3.5. Low Voltage Scanning Electron Microscopy (LVSEM)

Failure surfaces obtained after tensile tests were observed using an FEI XL-30 ESEM FEG scanning electron microscope at low accelerating voltage. The use of low voltage (between 0.8 kV and 1.4 kV) allows the observation of non-conductive samples without metal coating and thus the original sample surface characteristics are preserved.

4. Characterization results

For each chosen *processing temperature* (115 °C, 120 °C and 125 °C), several HVC experiments were performed at *total energies* ranging from 800 J/g to 4300 J/g. Cylinders of diameter 50 mm and around 10 mm height were obtained, which allows us to perform physical characterization (DSC and density measurements) and to machine specimens for mechanical characterization. For comparison, a melt-recrystallized UHMWPE was also investigated: Tivar® 1000 by Poly-HySolidur (Vreden, Germany). This semi-finished product is compression molded from GUR 4120 UHMWPE powder (molecular weight = 5×10^6 g/mol).

4.1. Physical characterization

It is of major importance to characterize the crystallinity, as it influences the mechanical properties. HVC UHMWPE crystal weight fractions were obtained from DSC experiments. DSC curves of nascent powder, melt-recrystallized UHMWPE and several HVC UHMWPE processed at 120 °C are presented in Fig. 4. As already noticed by other authors [14–16], nascent UHMWPE melting peak is around 142 °C (onset at 130 °C), while melt-recrystallized UHMWPE melting peak

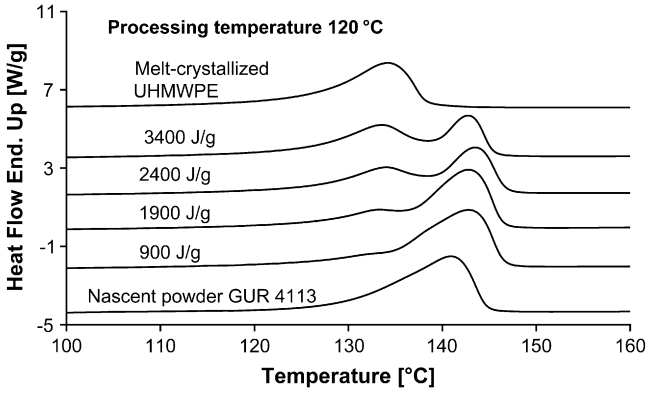

Fig. 4. DSC curves of HVC UHMWPE processed at 120 °C.

is around 135 °C (onset at 124 °C). As stated earlier in this paper, the origin of this phenomenon is not clear. However, it is a useful means to distinguish nascent and melt-recrystallized materials. HVC UHMWPE exhibits two melting peaks, revealing the presence of both nascent and melt-recrystallized materials. Two melting peaks have already been observed in UHMWPE, after annealing treatment of nascent powder, also owing to the presence of both nascent and melt-recrystallized materials [14,19,26].

The progressive appearance of the ''recrystallized'' peak with increasing *total energy* shows that there is a progressive partial melting of UHMWPE during HVC (Fig. 4). As melt-crystallized UHMWPE is less crystalline than nascent UHMWPE, partial melting comes with a progressive loss of crystallinity (see the plot of crystal weight fraction versus processing parameters in Fig. 5). The crystallinity degree not only decreases with *total energy* but also with *processing temperature*. The *processing temperature* appears to be a crucial parameter. For example, for a given *total energy*, a 5 °C increase in the *processing temperature* between 120 °C and 125 °C strongly decreases the crystallinity degree. However, as suspected, HVC UHMWPE crystallinity degree is always higher than melt-recrystallized UHMWPE one, due to the presence of nascent highly crystalline UHMWPE. In addition it is noted that increasing *processing temperature* shifts the appearance of partial melting toward low *total energy*. It can be seen by the beginning of the crystallinity drop, around 3000 J/g for processing at 115 °C, 2000 J/g for processing at 120 °C and 1000 J/g for processing at 125 °C.

A last comment can be made concerning the slight shift to high temperatures of the second melting peak with increasing energy (Fig. 4) and the slightly higher crystallinity of low compaction energy samples compared to the powder (Fig. 5). This could arise from crystal thickening by annealing, which is a classical mechanism in semi-crystalline polymers. However, after a 2 h annealing treatment at 120 °C, GUR 4113 powder melting peak is not changed, showing that this phenomenon is not only related to the temperature but also to the impacts.

Density measurements have been performed to evaluate material porosity. Indeed, a process implying particle sintering could lead to a porous material. It has been shown in a previous work [7] that insufficient *total energy* and resulting bad sintering, associated to thermal shrinkage, lead to a material with weak interfaces characterized by significant micro-porosity.

Fig. 6 presents densities versus processing parameters. These curves are tricky to analyze as UHMWPE intrinsic density depends on crystallinity degree that varies with processing parameters. To ease the interpretation, densities of Tivar® 1000 (UHMWPE obtained by compression molding) and calculated theoretical density for 70% crystalline UHMWPE have been added.

There is apparently little porosity below 1500 J/g, whatever be the *processing temperature*, however, above this energy, samples are fully dense. At low compaction energy, the opaque and white visual aspect of the samples is also a sign of pores' presence. This white aspect could be due to light scattering by cavities. The same phenomenon has been observed on POM processed by HVC [7] and is commonly observed during polymer plastic deformation [25]. The slight drop in density with increasing temperature and increasing energy above 2000 J/g is related to the crystallinity decrease (Fig. 5).

In short, the physical characterization has shown that HVC UHMWPE crystallinity degree (varying between nascent UHMWPE crystallinity (~70%) and melt-recrystallized crystallinity (~55%)) are governed by the processing parameters, and that above 1500 J/g HVC UHMWPE reaches full density.

4.2. Mechanical characterization

Three-point bending tests were performed to measure Young's modulus and to evaluate ductility. Results are plotted versus processing parameters in Fig. 7. The major result concerns ductility: while HVC POM has remained brittle for all processing conditions considered [7], HVC UHMWPE is ductile above: 1500 J/g for a *processing temperature* of 125 °C, 2500 J/g for a *processing temperature* of 120 °C and 3800 J/g for a *processing temperature* of 115 °C. Then, one can notice that HVC UHMWPE is stiffer than the conventionally processed sample (Tivar® 1000), nearly twice stiffer for certain processing conditions. This is not surprising considering the high crystallinity measured, due to the presence of a significant

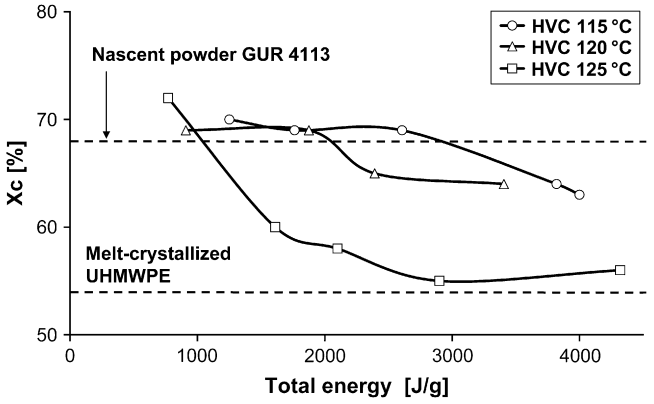

Fig. 5. Crystal weight fraction X_c from DSC versus *total energy* for three *processing temperatures*.

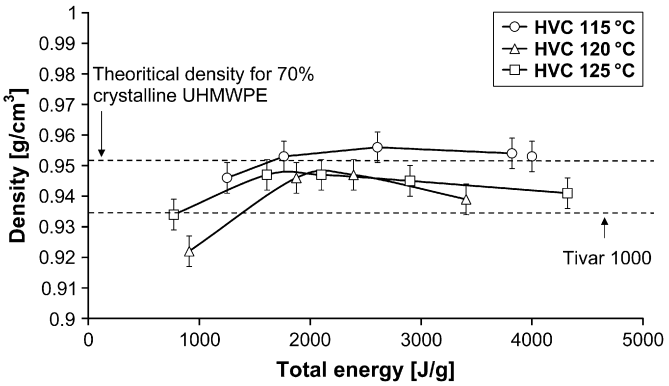

Fig. 6. Density versus *total energy* for three *processing temperatures*.

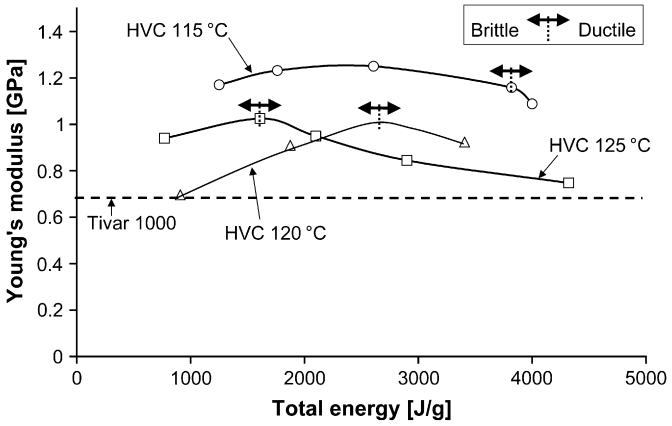

Fig. 7. Young's modulus and ductility from bending tests versus *total energy* for three *processing temperatures*.

fraction of nascent UHMWPE. Below 1500 J/g, a slightly lower modulus is observed, owing to little porosity. At higher *total energy*, Young's modulus reaches a maximum, and then began to drop. This drop is related to the drop in crystallinity due to partial melting/recrystallization of nascent UHMWPE. Above 2000 J/g, a significant drop of the modulus with the *processing temperature* is observed: the considerable influence of the *processing temperature* on partial melting and hence on crystallinity and modulus is confirmed.

In addition to bending tests, ductile samples were submitted to tensile tests, in order to investigate ultimate properties. Stress–strain curves of several samples are plotted in Fig. 8. Results on Young's modulus obtained by bending tests are confirmed, and HVC UHMWPE yielding properties appear to be interesting. Indeed, HVC UHMWPE yielding occurs always at higher stress than compression molded UHMWPE one. It could be due to the higher crystallinity degree of HVC UHMWPE and also perhaps thicker crystal lamellae with regard to numerous studies dealing with plastic deformation of polyethylene [9,27–31].

Then, tensile stress–strain curves clearly show that high fracture strains (up to more than 100% true strain) are reached when *processing temperature* and *total energy* are increased, but at the expense of modulus and yield stress. Fracture strain data have been plotted versus processing parameters in Fig. 9. For each sample, the values obtained over two or three tests do not differ more than 25% from their average value presented here. A good compromise between stiffness and ductility can be found at intermediate *processing temperature* and *total energy*. For example, at 3400 J/g and 120 °C, HVC UHMWPE has both a high stiffness and a high deformability (true strain between 20% and 40%).

To resume, for correctly chosen processing conditions, HVC leads to a fully dense bulk UHMWPE with a significant fraction of nascent material and very good mechanical properties including significant ductility and high stiffness. It confirms that HVC is a promising process. High Young's moduli and high yield stresses undoubtedly find their origin in the highly crystalline particular structure of the nascent UHMWPE. Qualitatively, considering only fully dense samples, processing parameters' influence is simple: an increase in *processing temperature* or *total energy* leads to more partial melting, which reduces Young's modulus and yield stress, but increases fracture strain.

5. Discussion

DSC shows the presence of both recrystallized and nascent materials in HVC UHMWPE and the sintering by fusion/recrystallization [7] suggests that the recrystallized material (forming local welds) would partially surround nascent particles: UHMWPE HVC can be seen as a bi-phased material of nascent and recrystallized UHMWPE at the micrometric scale.

UHMWPE HVC is therefore characterized by its recrystallized phase fraction, which can be evaluated by two different means, and it is possible to predict the Young's modulus by a parallel coupling model. Fracture surface observations have been performed in order to understand HVC UHMWPE fracture behavior, particularly the evolution of fracture strain with the fraction of recrystallized material.

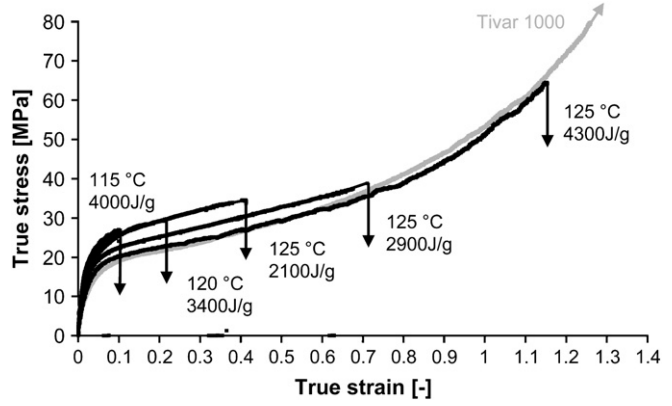

Fig. 8. Examples of true stress–true strain curves from tensile tests. Tivar® 1000 fails at approximately 1.5 true strain and 200 MPa true stress.

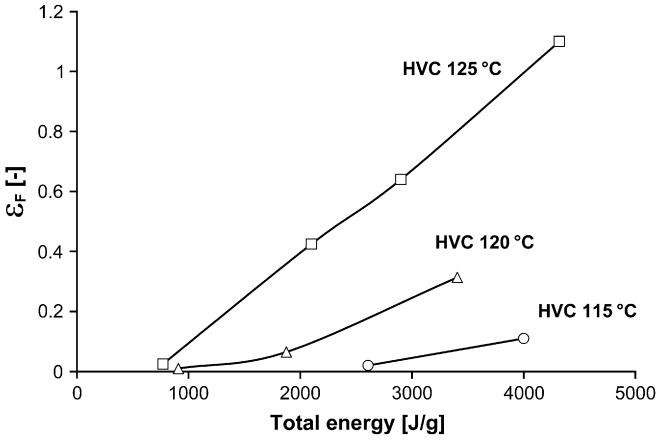

Fig. 9. Fracture strain average value ε_F versus *total energy* for three *processing temperatures*.

5.1. Recrystallized phase fraction

Two methods based on DSC results can be used to attain the recrystallized phase weight fraction f_R. By a mixing rule, it is first possible to obtain f_R from X_c, the overall crystal weight fraction, assuming the values of X_{c_R} and X_{c_N}, the crystal weight fractions within the recrystallized and nascent phases.

$$X_c = (1-f_R)X_{c_N} + f_R X_{c_R} \Leftrightarrow f_R = \frac{X_{c_N} - X_c}{X_{c_N} - X_{c_R}} \tag{4}$$

The following values are assumed for X_{c_R} and X_{c_N} : 54% and 71.5%, respectively. $X_{c_R} = 54\%$ is the value of the melt-recrystallized UHMWPE and $X_{c_N} = 71.5\%$ is the maximum crystallinity value measured, for a sample processed by HVC at 125 °C and 800 J/g. The precision on crystal weight fractions is ±0.01, so f_R is obtained with an accuracy of only ±0.1 to ±0.2. It leads us to try to reach f_R by an alternative method. Thanks to the double melting peak, it is possible to evaluate the enthalpies relative to the nascent and recrystallized phases by a deconvolution method. A satisfactory means to fit the melting peaks uses a combination of a Lorentzian function Eq. (5) until the maximum at $T = T_{peak}$ (left side of the peak), followed by a Gaussian function Eq. (6) (right side of the peak).

$$T \le T_{peak} \rightarrow f(T) = \frac{A \times \Gamma}{\left(T - T_{peak}\right)^2 + \left(\frac{1}{2}\Gamma\right)^2} + C \tag{5}$$

$$T > T_{peak} \rightarrow f(T) = \frac{B}{\sigma} e^{-\left(T - T_{peak}\right)^2 / 2\sigma^2} + C \tag{6}$$

A and B specify the peak amplitude and C the base line. Γ and σ are parameters specifying the width of the peak. An example of fitting by a least square method is provided in Fig. 10.

Then, to calculate f_R, one can express X_{c_R} and X_{c_N} as following:

$$X_{c_R} = \frac{m_R + m_N}{m_R}\frac{\Delta H_R}{\Delta H_{m0}} = \frac{1}{f_R}\frac{\Delta H_R}{\Delta H_{m0}} \tag{7}$$

$$X_{c_N} = \frac{m_R + m_N}{m_N}\frac{\Delta H_N}{\Delta H_{m0}} = \frac{1}{1-f_R}\frac{\Delta H_N}{\Delta H_{m0}} \tag{8}$$

m_R and m_N are the masses of recrystallized and nascent phases. ΔH_R and ΔH_N are the enthalpies of recrystallized and nascent phases, obtained by integration of the deconvoluted peaks' heat flow, and normalized by the sample mass $m_R + m_N$.

The value of ΔH_{m0}, the melting enthalpy of an infinite size crystal, is assumed to be the same for recrystallized and nascent phases, and finally:

$$f_R = \frac{\Delta H_R X_{c_N}}{\Delta H_R X_{c_N} + \Delta H_N X_{c_R}} \tag{9}$$

An advantage of the deconvolution method is that the precision of the crystal weight fraction has less influence on f_R accuracy. It depends much on the fitting used to calculate the enthalpies. It is thought that a relative precision of ±10% is obtained if the two peaks are well defined.

The results obtained by the two methods are given in Fig. 11. There is a satisfactory consistency between the two methods.

A jump in the recrystallized phase fraction is noted, around 1500 J/g for UHMWPE processed at 125 °C, 2500 J/g for UHMWPE processed at 120 °C and 3500 J/g for UHMWPE processed at 115 °C. This is the beginning of partial melting, which coincides with the crystallinity drop (Fig. 5) and the appearance of ductility (Fig. 7): it confirms that local melting is required to obtain particle welding and hence ductility.

5.2. Young's modulus prediction

In order to attempt to predict the modulus of semi-crystalline polymers, nanoscale microstructural models are generally used [9,32–34]. Unfortunately, crystal modulus and amorphous modulus are difficult to determine, in particular amorphous modulus is known to vary with crystallinity (confinement effect) [9]. For HVC UHMWPE, two phases are present at the micrometric scale, the nascent one and the recrystallized one. Both phases are formed of semi-crystalline

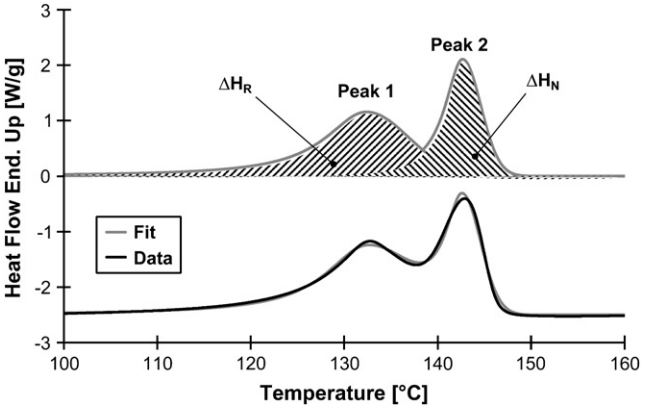

Fig. 10. Example of DSC curve fitting used to calculate the recrystallized phase fraction f_R.

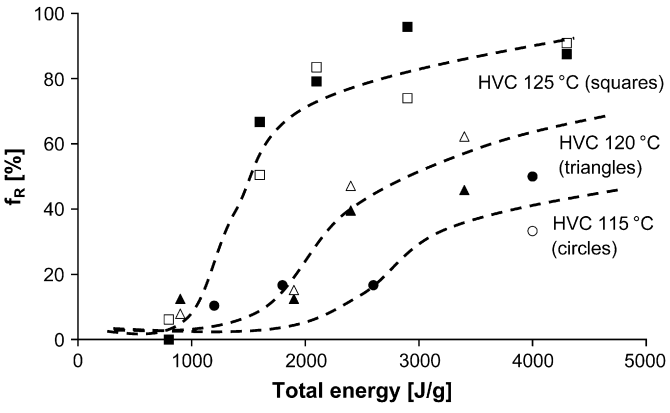

Fig. 11. Recrystallized phase fraction f_R versus processing parameters. Filled symbols = "X_c method" and open symbols = "deconvolution method".

material, but with different crystallinities. The nascent phase has a higher crystallinity degree than the recrystallized phase, imparting to it a higher modulus.

In the case of HVC UHMWPE, it appears more convincing to adopt a two phase model at the micrometric scale than at the nanometric scale, as it is closer to the HVC UHMWPE morphology. The plot of Young's modulus versus recrystallized phase volume fraction ϕ_R (Fig. 12) shows that a simple parallel model at the micrometric scale predicts its evolution.

The phase volume fraction ϕ_R is calculated, from an average value of f_R over the two methods, as follows:

$$\phi_R = \frac{f_R \rho_N}{\rho_R - f_R(\rho_R - \rho_N)} \tag{10}$$

with $\rho_N = 0.953$ ($X_c = 71.5\%$) and $\rho_R = 0.927$ ($X_c = 54\%$).

Only the Young's moduli of the fully dense samples (compacted over 2000 J/g) are plotted. The melt-recrystallized UHMWPE value, situated at $\phi_R = 1$, is included.

One can remark that the points approximately follow a straight line. This line stands for the parallel mechanical coupling of the nascent and recrystallized phases. The nascent phase Young's modulus, obtained by extrapolation, is 1.35 GPa, which is approximately twice the melt-recrystallized value. As there is only a little difference between the moduli of the two phases, the parallel model gives a satisfactory prediction of the modulus, and a more elaborated model (Takayanagi model [8] for example) is not needed.

5.3. Fracture behavior

In this part of the discussion, fracture behavior is analyzed in relation with the microstructure. Tensile tests show that fracture strain increases with *processing temperature* and *total energy*, hence with recrystallized phase fraction. As it has been done for the Young's modulus, the fracture strains are plotted versus recrystallized phase fractions in Fig. 13. Even if ductility is quickly reached, a high proportion of recrystallized phase is needed to reach significant deformation (40–50%). Fracture surfaces of three samples, marked (A), (B) and (C) in Fig. 13, were observed by LVSEM in order to understand

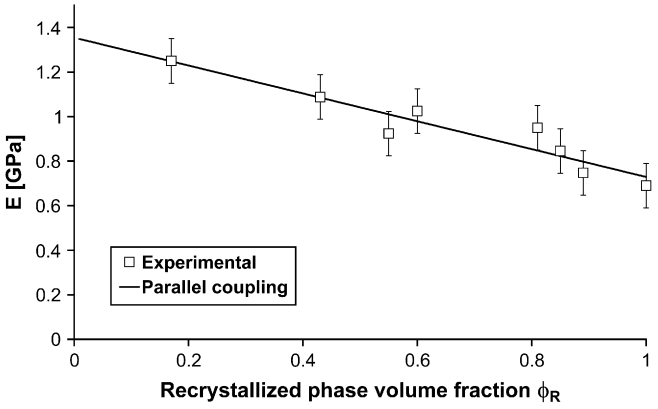

Fig. 12. Young's modulus versus recrystallized phase volume fraction: experimental values and parallel coupling model.

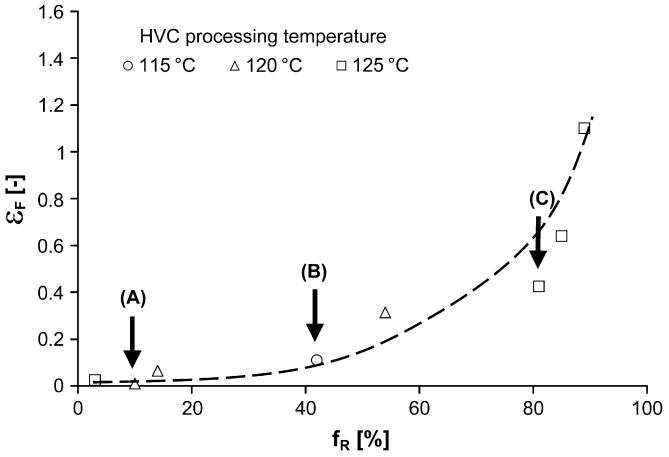

Fig. 13. Fracture strain versus recrystallized phase fraction. The samples observed by LVSEM are pointed by an arrow.

large deformation mechanisms and fracture behavior. Sample A is brittle, sample B has failed around 10% strain and sample C around 40% strain.

As observed in Fig. 14, brittle sample A exhibits an interparticle failure with several open interfaces (pointed by an

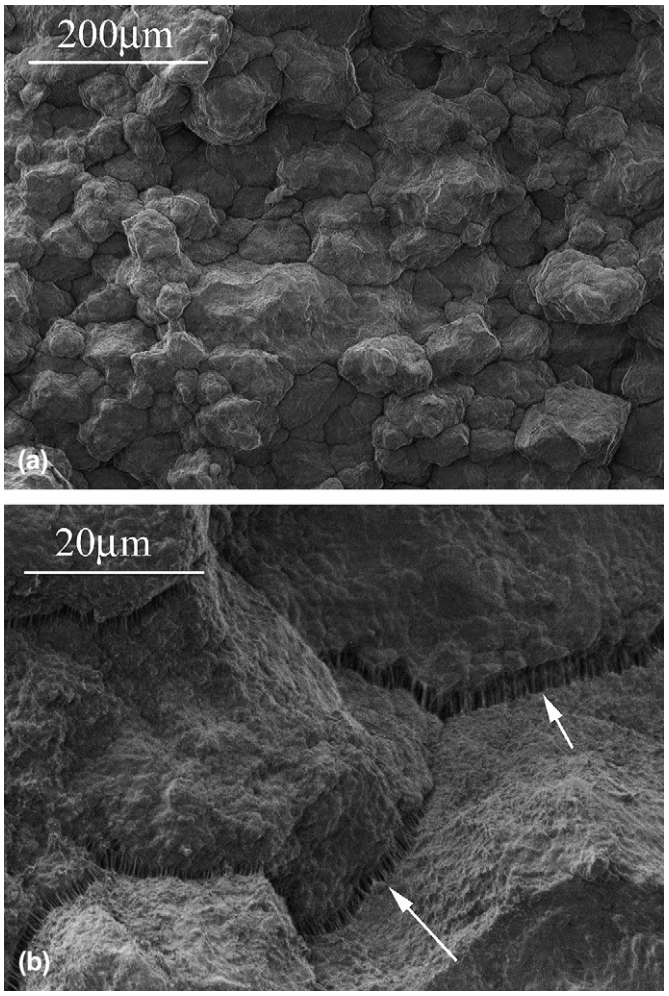

Fig. 14. LVSEM fracture surface observation of brittle sample A. (a) Interparticle failure. (b) The arrows show weak interfaces between particles.

arrow in Fig. 14b). These weak interfaces exhibit nano-fibrils (~100 nm) very similar to the ones observed within certain samples of POM processed by HVC. As for POM, it is thought that nano-fibrils and pores have not been formed during the mechanical testing, but during cooling, owing to an inhomogeneous thermal retraction [7]. The presence of open interfaces is consistent with density measurements showing that samples are slightly porous at low *total energy* (Fig. 6). Fibrils are too weak to ensure a good cohesion between the particles and to permit their deformation, explaining the brittle inter-particle failure.

On ductile samples' fracture surfaces (B and C), initial particles are more difficult to distinguish (see Fig. 15a and white points in Fig. 16a), but the failure appears to be also interparticular. Contrary to brittle samples, no open interfaces are noticed, suggesting that there are strong links between the particles. Numerous micro-fibrils (~1 μm, see Fig. 15b) are observed on particle surfaces. The inter-particle character of the failure and the presence of micro-fibrils are consistent with the idea that the recrystallized material is located mainly at particle interfaces owing to sintering by melting/recrystallization [7]. As recrystallized material's yield stress is lower than the nascent one (see tensile test results in Fig. 8), the plastic deformation preferentially occurs in the recrystallized phase during the mechanical testing. Then, when recrystallized material reaches its maximum extension, the failure occurs between the nascent particles, revealing an inter-particle and fibrillar failure surface. Consequently, the nascent phase has not been significantly deformed, explaining that the fracture strains of HVC UHMWPE are lower than the melt-recrystallized UHMWPE ones.

In Fig. 16 (sample C), in addition to micro-fibrils, some very thick fibrils (10–30 μm) are observed (indicated by arrows). These fibrils originate in the stretching of large zone of melt-recrystallized UHMWPE. This is consistent with both the high recrystallized phase fraction (~80%) and the high fracture strain (~0.4) measured on this sample.

Finally, it is noted that large deformations are accompanied by extensive cavitation, as a significant whitening of the samples has been observed. Cavitation, as plastic deformation, probably occurs preferentially at particle interfaces.

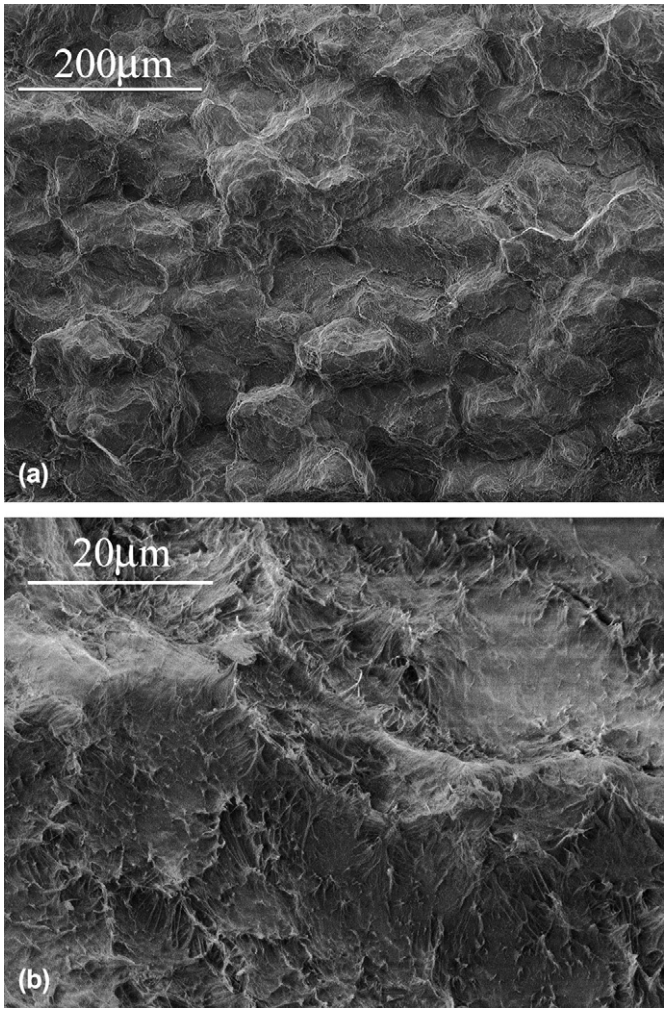

Fig. 15. LVSEM fracture surface observation of ductile sample B. (a) Inter-particle failure. (b) Characteristic micro-fibrillar surface.

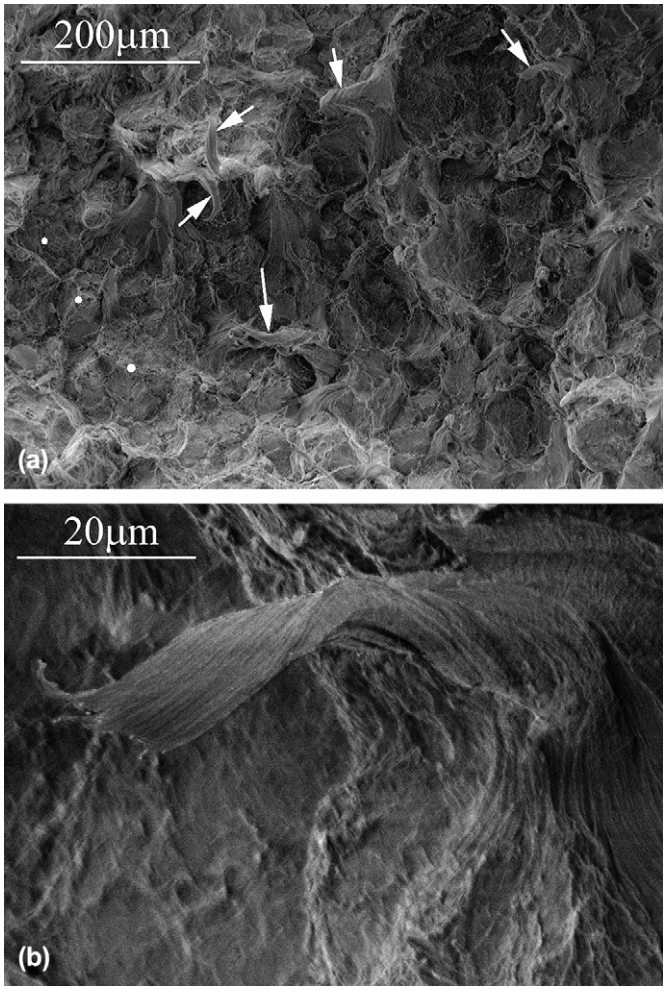

Fig. 16. LVSEM fracture surface of ductile sample C. (a) The circles help to distinguish different particles and the arrows show thick fibrils. (b) Detail of a "thick" fibril.

In light of this discussion, it appears that

- HVC UHMWPE is formed of stiff nascent particles surrounded by melt-recrystallized material matrix ensuring the material cohesion;
- the fraction of melt-recrystallized material (governed by the processing parameters) influences material properties, in particular the modulus, yield stress and fracture strain.

6. Conclusion and prospects

As a conclusion, UHMWPE nascent powder was successfully processed by HVC. UHMWPE processed by HVC reveals to be ductile and exhibits higher Young's modulus and yield stress than conventionally processed UHMWPE. In addition, the processing times are advantageous: a few minutes versus several hours for conventional processing of UHMWPE. Very good elastic properties originate in the high crystallinity of nascent UHMWPE powder that is partially preserved by the process.

A fraction of nascent UHMWPE is melted during HVC and the mechanical properties of HVC UHMWPE are strongly influenced by the resulting fraction of melt-recrystallized material. Low recrystallized phase fraction favors the stiffness at the cost of ultimate properties whereas high recrystallized phase fraction favors the ultimate properties at the cost of stiffness. Mechanical properties are hence adjustable according to a given application.

It is assumed that sintering occurs thanks to local melting/recrystallization at particle interfaces, inducing a microstructure composed of nascent highly crystalline particles surrounded by a melt-recrystallized material. Fracture surface observations support this scenario. More investigation on sintering mechanisms and microstructure is needed to confirm and detail this scenario.

With the use of HVC, which preserves the nascent high crystallinity of UHMWPE, crucial properties for biomedical applications in total joint prostheses, such as wear and creep resistance, should be improved. These properties need to be investigated in order to consider HVC UHMWPE for use in orthopedic implants [35].

References

[1] Kelly JM. Journal of Macromolecular Science, Part C: Polymer Reviews 2002;42:355–71.
[2] Truss RW, Han KS, Wallace JF, Geil PH. Polymer Engineering and Science 1980;20:747–55.
[3] Parasnis NC, Ramani K. Journal of Materials Science: Materials in Medicine 1998;9:165–72.
[4] Gul RM, McGarry FJ. Polymer Engineering and Science 2004;44:1848–57.
[5] Azhdar B, Stenberg B, Kari L. Polymer Testing 2005;24:909–19.
[6] Jauffres D, Lame O, Vigier G, Lazzarotto L, Chervin C. High velocity die compaction: application to polymer processing. In: Proceedings of the 4th international conference on science, technology and application of sintering. Grenoble: Institut National Polytechnique de Grenoble; 2005. p. 95–8.
[7] Jauffres D, Lame O, Vigier G, Doré F, Chervin C. Journal of Applied Polymer Science 2007;106:488–97.
[8] Ward IM, Sweeney J. Mechanical properties of solid polymers. London: Wiley; 2004.
[9] Crist B, Fisher CJ, Howard PR. Macromolecules 1989;22:1709–18.
[10] Farrar DF, Brain AA. Biomaterials 1997;18:1677–85.
[11] Shen DW, McKellop HA, Salovey R. Journal of Biomedical Materials Research 1998;41:71–8.
[12] Gao P, Cheung MK, Leung TY. Polymer 1996;37:3265–72.
[13] Kurtz SM, Muratoglu OK, Evans M, Edidin AA. Biomaterials 1999;20:1659–88.
[14] Wang XY, Salovey R. Journal of Applied Polymer Science 1987;34:593–9.
[15] Hofmann D, Schulz E, Fanter D, Fuhrmann H, Bilda D. Journal of Applied Polymer Science 1991;42.
[16] Tervoort-Engelen YMT, Lemstra PJ. Polymer Communication 1991;32:343–5.
[17] Morin FG, Delmas G, Gilson DFR. Macromolecules 1995;28:3248–52.
[18] Cook JTE, Klein PG, Ward IM, Brain AA, Farrer FD, Rose J. Polymer 2000;41:8615–23.
[19] Phillips RA. Journal of Polymer Science, Part B: Polymer Physics 1998;36:495–517.
[20] Rastogi S, Lippits DR, Hohne GW, Mezari B, Magusin PCMM. Journal of Physics: Condensed Matter 2007;19:205122.
[21] Mandelkern L. The crystalline state, Physical properties of polymers. Washington: ACS Books; 1993. p. 145–200.
[22] Brandrup J, Immergut EH, Bloch DR, Gruckle EA. Polymer handbook. New York: Wiley; 1999.
[23] Kong Y, Hay JN. Polymer 2002;43:3873–8.
[24] ASTM. Standard D790: test method for the flexural properties of unreinforced and reinforced plastics and electrical insulation materials, Annual book of ASTM standards. Philadelphia: American Society for Testing and Materials; 1999. p. 269–78.
[25] Quatravaux T, Elkun S, G'Sell C, Cangemi L, Meimon Y. Journal of Polymer Science, Part B: Polymer Physics 2002;40:2516–22.
[26] Sharma KG. Easily processable ultra high molecular weight polyethylene with narrow molecular weight distribution. Eindhoven: Technische Universiteit Eindhoven; 2005. p. 117.
[27] Kennedy MA, Peacock AJ, Mandelkern L. Macromolecules 1994;27:5297–310.
[28] Gaucher-Miri V, Seguela R. Macromolecules 1997;30:1158–67.
[29] Brooks NWJ, Mukhtar M. Polymer 2000;41:1475–80.
[30] Schrauwen BAG, Jansen RPM, Govaert LE, Meijer HEH. Macromolecules 2004;37:6069–78.
[31] Oleinik EF. Polymer Science Series C 2003;45:17–117.
[32] Guan X, Pitchumani R. Polymer Engineering and Science 2004;44:433–51.
[33] Janzen J. Polymer Engineering and Science 1992;32:1242–54.
[34] Doyle MJ. Polymer Engineering and Science 2000;40:330–5.
[35] Jauffrès D, Lame O, Vigier G, Fridrici V, Doré F, in press.